ADVANCED OPTICAL MATERIALS
www.advopticalmat.de

Real-Time Tuning Exciton-Plasmon Coupling with Photosensitive Nanocavity

Xiaobo Han, Zijian He, Dong Zhao, Huatian Hu, Shujin Li, Meng Yuan, Kai Wang,* and Peixiang Lu**

A novel method is proposed to directly characterize the exciton-plasmon coupling in a photosensitive nanoparticle-on-mirror (NPoM) nanocavity. Under the illumination of UV light, the localized surface plasmon resonance (LSPR) peaks of the nanocavity can be continuously tuned over a wide range (≈65 nm), enabling precise determination of the energy dispersion relationship of plexcitons in the nanocavity. The results indicate that the energy of Rabi splitting can be actively tuned from 65 meV (weak coupling) to 170 meV (strong coupling) by adjusting the LSPR peak of a specific nanocavity (particle size *L*≈55-92 nm) to the exciton wavelength (the zero detuning). In addition, the criterion of strong coupling is optimized by introducing single-particle absorption spectroscopy. The work offers an intuitive method for the strong coupling characterization in nanocavity, paving the way for the real-time tuning of coupling strength over a wide range (100 meV) from weak to strong coupling regimes.

1. Introduction

Manipulating the optical properties of semiconductors by the localized surface plasmons (LSPs) in noble metal nanostructures continues to be a fascinating and active area in nanophotonic research. Of particular interest is the interaction between LSPs and excitons under resonant conditions,[1] which can be divided into the weak and strong coupling. In the weak coupling regime, the spontaneous emission rate can be enhanced due to the modified photonic density of state (Purcell factor), which has been widely applied in nanophotonic devices and biosensing applications.[2,3] More attractive change in emission characteristics occurs when the strong coupling condition is satisfied.[4–6] New hybrid light-matter states emerge with a characteristic energy difference known as Rabi splitting ($\hbar\Omega$), where energy is repeatedly exchanged between excitons and plasmons. Thus, the shifted energy of the new states relative to the exciton energy can be controlled by changing the coupling strength, and then many attractive phenomena can be realized, such as nonlinear polaritons, extremely long energy transfer processes, and chemical reactivity modifications.[7–11] Hence, the active tuning of the coupling strength from weak to strong coupling in an exciton-plasmon system draws lots of attention. Previously, it was demonstrated to actively tune the coupling strength by controlling exciton density, such as electricity and solution, which is limited by a relatively narrow range.[12–17]

Alternatively, lots of works present the tuning of coupling strength by engineering the LSPs in plasmonic nanostructures with different sizes and shapes.[18–21] However, it usually requires the complicated fabrication of plasmonic structures with different parameters to establish exciton-plasmon hybridization, which can easily introduce experiment deviations and errors. In particular, the characterization of the exciton-plasmon coupling in a nanocavity is actually based on a multi-nanocavity measurement.[22–30] One has to repeatedly measure the scattering spectra from many different nanocavities for the energy dispersion relationship of the plexciton in nanocavity. It relies on the assumption that the multi-nanocavity only introduces the different detuning energies between the excitons and LSPs, while keeping other parameters (mode volume, exciton number, and even exciton property) constant. Therefore, from a more rigorous perspective, the former statistical characterization of strong coupling still needs further verification. However, it is quite challenging to actively manipulate the detuning energy between the LSPs and excitons in an individual nanocavity. To the best of our knowledge, only one previous work reported the characterization

X. Han, H. Hu
Hubei Key Laboratory of Optical Information and Pattern Recognition
Wuhan Institute of Technology
Wuhan 430205, China
Z. He, S. Li, M. Yuan
School of Physics
Huazhong University of Science and Technology
Wuhan 430074, China
D. Zhao, K. Wang
School of Electronic and Information Engineering
Hubei University of Science and Technology
Xianning 437100, China
E-mail: zhaodong@hbust.edu.cn
K. Wang, P. Lu
Wuhan National Laboratory for Optoelectronics
Huazhong University of Science and Technology
Wuhan 430074, China
E-mail: kale_wong@hust.edu.cn; lupeixiang@hust.edu.cn
P. Lu
Guangdong Intelligent Robotics Institute
Dongguan 523808, China

The ORCID identification number(s) for the author(s) of this article can be found under https://doi.org/10.1002/adom.202301553

DOI: 10.1002/adom.202301553

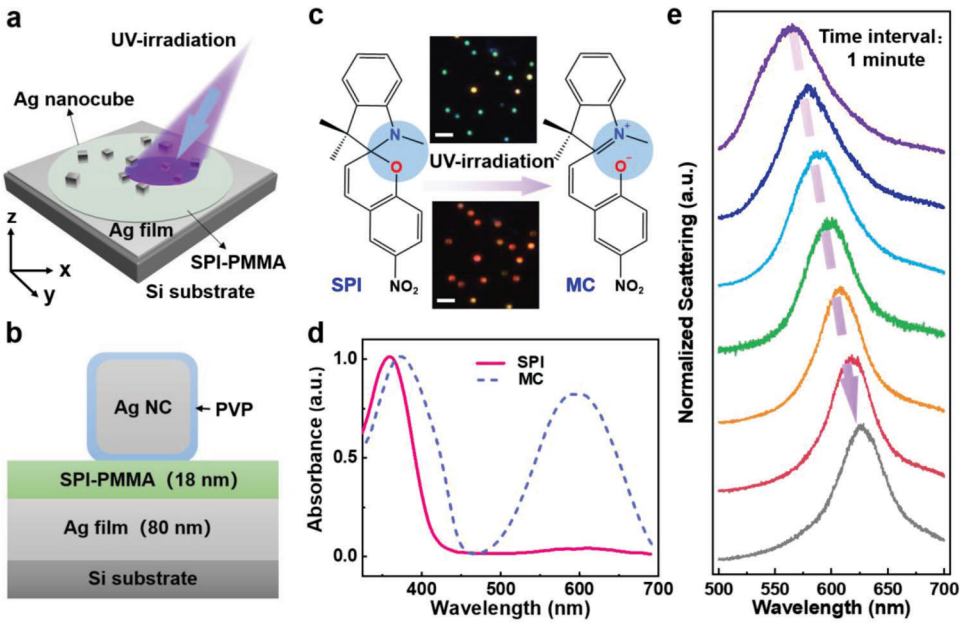

Figure 1. a,b) Schematic of the Ag nanocavity consisting of a Si substrate, an 80-nm thick Ag film, an 18-nm-thick SPI-PMMA layer and Ag NCs (coated with 3-nm thick PVP) in different sizes. An oblique UV light is used to excite the hybrid nanocavity. c) Changes of the chemical structure of photochromic molecules under UV illumination (from SPI to MC) and corresponding dark-field scattering images (from top to bottom). Scale bars are 5 μm. d) Absorption spectra of the SPI-PMMA in anisole before (purple "SPI") and after UV irradiation (light blue "MC"). e) Normalized dark-field scattering spectra of the Ag nanocavity from the same NC. Increased with the UV irradiation duration, the LSPR peaks gradually redshift.

based on a nanocavity, tuning the LSPs peaks by repeatedly depositing alumina onto the plasmonic particles.[31,32] Therefore, it is still urgent to develop a simple and easy-to-control method to characterize the energy dispersion relationship of the plexciton in an individual nanocavity.

In this letter, we propose a photosensitive plasmonic nanocavity to realize the direct characterization of the exciton-plasmon coupling. Exploiting a photosensitive spacer of the photochromic molecule, the LSPs peak of the nanoparticle-on-mirror (NPoM) nanocavity can be continuous tuning over 65 nm with UV light illumination. Therefore, the energy dispersion relationship of the plexcitons in an individual nanocavity can be achieved directly, excluding any deviations caused by multi-nanocavity. Furthermore, the results indicate that the energy of Rabi splitting can be actively tuned from 65 meV (weak coupling) to 170 meV (strong coupling) by shifting the LSPR peak of a specific nanocavity (particle size $L \approx$55–92 nm) to match with the exciton wavelength (610 nm, WS_2 monolayer). In addition, the strong coupling criterion is further optimized by combining the single-particle absorption and scattering spectra. Our work provides an in situ and all-optical method for studying the exciton-plasmon coupling in an individual nanocavity, presenting the continuous tuning of coupling strength over a wide range (up to 105 meV) from weak to strong coupling regimes.

2. Results and Discussion

Plasmonic nanocavity consisting of single nanoparticles (NPs) has drawn lots of attention. Especially, the NPoM nanocavity possesses a large electric field and tiny mode volume.[27] It provides a superior platform for strong coupling research.[32,33] The nanogap (spacer) in the plasmonic nanocavity shows a unique feature, which can act as an LSPR adjuster by changing its thickness. Usually, the spacer is made of oxides, such as alumina, or polymer.[34,35] Interestingly, when the polymer is chosen, various materials such as dyes can be doped. Photochromic molecule means that by excitation at specific wavelengths, compounds can undergo specific chemical reactions to change the structure and the absorption spectrum. Thus, the spacer doped with a photochromic molecule can act as a real-time LSPR adjuster under light conditions, which has been shown in various nanocavities, such as nanodisk arrays.[36–43] In this work, as shown in **Figure 1**a,b, the plasmonic cavity uses noble metal Ag as the basic material for building the cavity, and the SPI-polymethyl methacrylate (PMMA) film is selected as the spacer. SPI is one of the organic photochromic materials, and absorption occurs in the UV region. Ag nanocubes (Ag NCs, nanoComposix) are then dispersed on the spacer, where Ag NCs were coated with a 3-nm thick Polyvinylpyrrolidone (PVP). Detailed sample preparation is provided in the Supporting Information.

Figure 1c shows the chemical structure of the photochromic isomer before (SPI) and after (MC) UV irradiation, indicating a C —O ring opening reaction. To understand the photoisomerization process, the absorption spectra of SPI-PMMA in anisole were tested by a UV/vis spectrophotometer. In Figure 1d, the absorption spectrum before UV irradiation (labeled SPI) shows only one distinct peak at ≈360 nm and the solution appear transparent, while the spectrum after UV irradiation (labeled MC) shows a new significant peak at ≈600 nm, and the solution appears blue-purple. According to previous work,[36] a large increase in the absorption peak at 600 nm during photochromism implies a change in the refractive index of the spacer. It causes

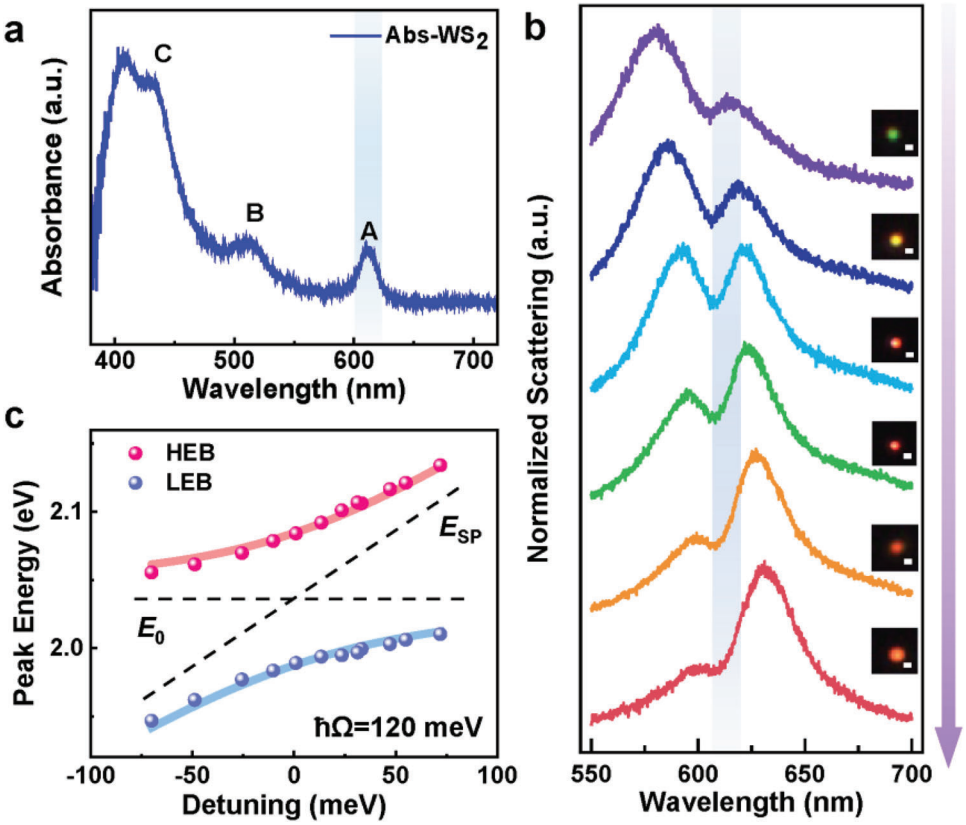

Figure 2. a) Absorption spectrum of WS_2 monolayer on the SPI-PMMA/Ag film. The light blue region indicates the A exciton. b) Normalized dark-field scattering spectra of WS_2 monolayer-Ag nanocavity from the same NC. The position of the blue area corresponds to the exciton wavelength. Under UV irradiation, the spectra are redshift (from top to bottom). Insets show the corresponding scattering images of the measured particle. Scale bars are 1 μm. c) The extracted energy peaks as a function of detuning from Figure 2b. The black dashed lines represent the plasmonic resonance E_{SP} and the exciton energy E_0, respectively. Dots represent the experimental data, and the solid curves are the fitting results. The Rabi splitting energy is 120 meV.

most of the particles in nanocavities to change from green to red after UV irradiation as shown in the scattering images in Figure 1c. Specifically, the normalized scattering spectra of a fixed particle under UV irradiation for different durations are shown in Figure 1e. The LSPR is actively and continuously tuned from 565 (green) to 630 nm (red), corresponding to a range of 65 nm. Therefore, the controllable optical properties of SPI-PMMA films make them ideal candidate for altering the nanocavity resonance.

Based on the above tuning method, it can be extended to the strong coupling measurement. To match the wavelength (≈600 nm) of the change in the refractive index of the photochromic molecule, WS_2 monolayer is selected. **Figure 2**a shows the absorption spectrum of WS_2 monolayer (purchased from Six-carbon Tech. Shenzhen) on a SPI-PMMA/Ag film. The A-exciton is located at 610 nm, according with the interested band, and the decay line widths (γ_0) is 70 meV. To demonstrate the UV light tuning process, we measure the scattering spectra of multiple particles as a function of UV irradiation duration. The typical scattering spectra of UV light tuning are shown in Figure 2b. Insets show the corresponding scattering images, and wide-field views can be seen in Figure S2 (in Supporting Information). With the redshift of the LSP peak, the scattering color of the particle accordingly varies from green to yellow and then to red. All spectra show one distinct dip and two peaks. The dip position is fixed and corresponds to the exciton wavelength. The split scattering spectra are characteristic features of plexcitons, a manifestation of the hybridization between plasmons and excitons. And the spectral shift behavior is consistent with the previous strong coupling results.[12,23,25,32] It confirms that the coupling effect is not affected by the photochromic molecule, except for the shift of the plasmonic resonance.

The coupling between excitons and plasmons can be described by a semiclassical coupled harmonic oscillator model, with the energies of the two splitting modes (hybrid states) given by

$$E_{\pm} = \frac{1}{2}\left(E_{SP} + E_0 \pm \sqrt{4g^2 + \delta^2}\right) \quad (1)$$

where E_{SP} and E_0 are the resonant energies of uncoupled plasmons and excitons, respectively; $\delta = E_{SP} - E_0$, said detuning; g is the coupling strength between plasmons and excitons. Figure 2c shows the extracted energy peaks as a function of detuning from Figure 2b, which clearly exhibits an anticrossing behavior (data analysis is detailed in Supporting Information). The peak energies above (or below) the exciton transition energy are simply defined as the high (or low) energy branch (HEB or LEB). The two solid curves fitted by equation Equation (1), represent the

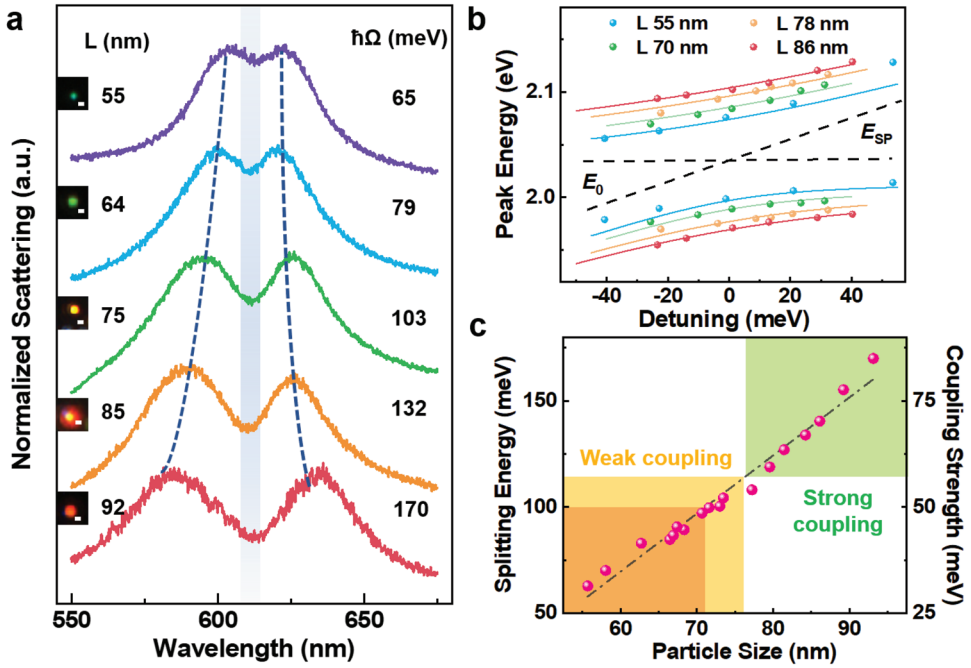

Figure 3. a) Scattering spectra at zero detuning from different size particles. The blue dashed curves are a guide for the eye showing the variation trend of peak energies. Insets show the scattering images of NCs before UV irradiation and the particle sizes. The values on the right are the corresponding Rabi splitting energy. Scale bars are 1 μm. b) Dispersion curves with different size particles. Dots represent the experimental data, and the solid curves are the fitting results. c) Rabi splitting (coupling strength) as a function of particle size varying from 55 to 92 nm.

dispersion relation of the two hybrid states. The splitting energy is derived to be $\hbar\Omega = 2g = 120$ meV. Since $\gamma_{SP} \approx 155$ meV and $\gamma_0 \approx 70$ meV in Figure S3 (Supporting Information), the strict criterion for strong coupling $\hbar\Omega > \frac{\gamma_{SP} + \gamma_0}{2} \approx 112$ meV is satisfied. It is noted that the average goodness of fit (R^2) by Equation (1) is better than that from the data from traditional multi-nanocavity (details are shown in Supporting Information).[27] Figure S4 (Supporting Information) shows the fitting results of multiple sets of data, indicating that the fitting accuracy is significantly improved from 0.77 to 0.98. It means that the non-uniformity of the nanocavity quality, the variation of exciton number and mode volume of multi-cavity have a great influence on the accuracy of coupling strength. Additionally, we know that mode splitting can also be measured from a plasmonic cavity of irregular shaped particles, and this platform can completely shield the uncertainty. Therefore, we develop a highly accurate, convenient and all-optical approach of measuring dispersion relation in individual nanocavities.

By adjusting the UV illumination duration, the LSPR peaks of each hybrid cavity can be tuned to the exciton wavelength, namely zero detuning. **Figure 3**a shows a series of scattering spectra of different size particles at zero detuning. Note that all data are measured at the same thickness spacer. Ag NC sizes (L) with the initial scattering images are listed in the left panel. Ag NC sizes are estimated by their corresponding LSPR peaks before UV irradiation in Figure S5 (Supporting Information).[44] It can be seen that as the particle size increases, the splitting energy increases from 65 to 170 meV, resulting in a giant tuning range of up to 105 meV at ambient condition. Also, Figure 3b presents the dispersion curves with different size particles. The splitting energy of 55, 70, 78, and 86 nm particles are 68, 95, 117, and 135 meV, respectively. Consistent with the trend shown in Figure 3a, it indicates that the splitting energy increases as the particle size increases. Note that the exciton transition energy of WS_2 slightly deviates in different batches. Thus, the orange data in Figure 3b is shifted 19 meV (6 nm in wavelength) along the y-axis for comparison convenience. In addition, the splitting energy obtained by the peak energy difference at zero detuning is similar to that by fitting the anticross curves. Thus, given the advantages of a highly accurate method, the splitting energy can be directly estimated from the peak energy difference at zero detuning rather than from the fitting of dispersion curves.

To reveal the effect of particle size on the coupling system, the splitting energy and coupling strength of different size particles are studied as shown in Figure 3c. Intuitively, the splitting energy is a linear function of particle size ($2g \propto L$), which is consistent with the previous work.[32] Note that there are both weak and strong coupling within the wide tuning range. According to rigorous criterion of strong coupling ($\hbar\Omega > \frac{\gamma_{SP} + \gamma_0}{2}$), hybrid nanocavities consisted of particles >76 nm (green area in Figure 3c can achieve strong coupling. To reveal the physical mechanism of splitting energy variation with particle size, the coupling strength can be calculated as:

$$g = \mu_m \sqrt{\frac{4\pi\hbar N c}{\lambda \varepsilon \varepsilon_0 V}} \tag{2}$$

where μ_m is the exciton transition dipole moment of WS_2 monolayer, N and λ are the number and wavelength of the exciton,

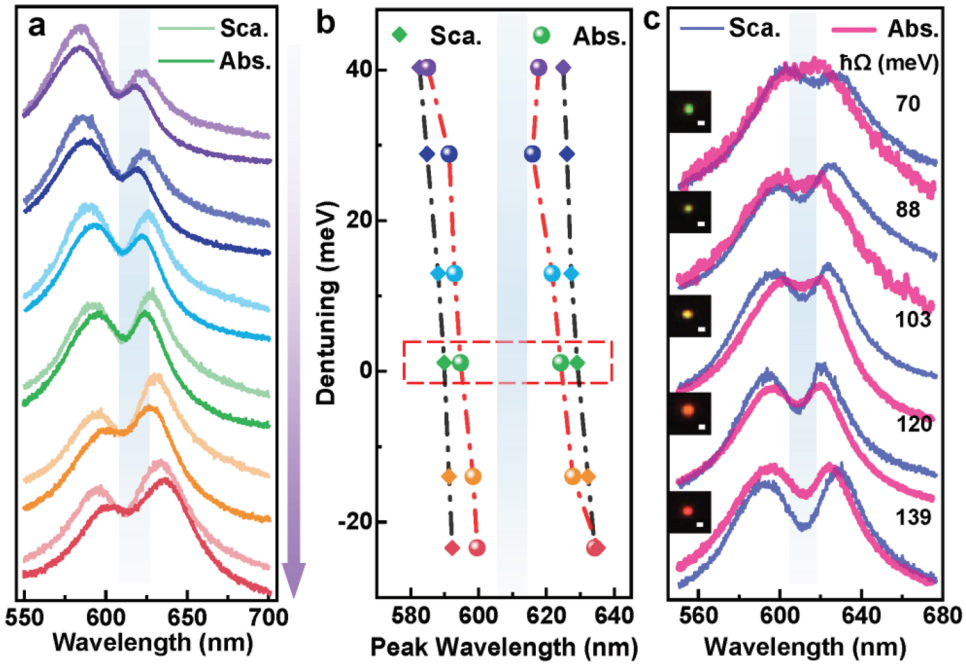

Figure 4. a) Time-dependent scattering and absorption spectra from the same NC under UV irradiation. The time is scanned in 1 min steps. b) Detuning-dependent peak wavelengths of scattering (rhombus) and absorption (spheres) extracted from Figure 4a. The red rectangle marks the data near zero detuning. c) Absorption and corresponding scattering spectra from different size particles. Insets show the scattering images of NCs before UV irradiation. Scale bars are 1 μm.

ϵ is the dielectric function. V is the effective mode volume of the nanocavity. The relationship between coupling strength and NC size is shown in Figure 3c ($2g \propto L$). It means that within the NC size ranging from 55 to 92 nm, the coupling strength can be tuned by particle size, and the exciton number increases dramatically at the same time. Note that the hybrid cavity of a larger particle ($L > 92$ nm) means that the exciton energy is initially crossed ($E_{SP} > E_0$). In other words, the corresponding detuning $\delta = E_{SP} - E_0$ is always positive and does not cross the zero detuning, so at the current spacer thickness, a larger particle size is not compatible.

Dark-field scattering technique is the most commonly used characterization method in hybrid nanocavities,[45] and most of the strong coupling work is only verified by this method. However, mode splitting in scattering spectra can be caused by two mechanisms: Rabi splitting at strong coupling and Fano resonance at weak coupling.[15,26,33,46–48] Therefore, it is still questionable to determine the strong coupling from scattering results alone. The absorption spectrum is considered a more accurate method. Thus, the continuous tuning process of scattering and absorption spectra under UV irradiation are shown in **Figure 4**a. Details about the optical measurements can be found in Supporting Information. From top to bottom, the scattering and absorption spectra have the same trend, while the peak positions and the dip depth show obvious deviations. Specifically, HEB and LEB of scattering and absorption spectra are extracted respectively, and the detuning is taken as the ordinate to obtain Figure 4b. Clearly, the energy splitting of absorption spectra at any detuning is smaller than that of scattering spectra. At near zero detuning, the calculated splitting energies are 117 and 98 meV, respectively. A difference of ≈20 meV implies the effect of plasmon dissipation, which is an important factor affecting the judgment of strong coupling. Thus, the tuning process can be characterized by scattering and absorption spectra, and the strong coupling criterion can be optimized here.

At present, the commonly used strong coupling criterion has the following two formulas: loose one: $\hbar\Omega > \frac{\gamma_{SP} - \gamma_0}{2}$ and strict one: $\hbar\Omega > \frac{\gamma_{SP} + \gamma_0}{2}$. In our experiment, the values calculated are 42 and 112 meV, respectively. Obviously, a huge numerical difference causes the boundary between strong and weak coupling to be blurred. The synergistic contribution of scattering and absorption spectra at zero detuning provides a good opportunity to optimize the criterion. In Figure 4c, the absorption and scattering spectra of different size particles are presented. According to absorption spectra, $\hbar\Omega = 103$ meV can be roughly regarded as a dividing line, because spectra with $\hbar\Omega < 103$ meV have no dip, and those with $\hbar\Omega > 103$ meV have distinct dips. In the scattering spectra, however, $\hbar\Omega = 70$ meV still shows a dip. It is considered that contributions of exciton and plasmon losses to spectral splitting affect both the absorption and scattering spectra, while the absorption one is less affected.[49] Thus, there are deviations between common criteria and experimental results. Especially, when the loose condition is applied, simple spectral broadening or Fano resonance may be mistaken for reaching the strong coupling mechanism. Here, according to the above experimental results, the following formula, $\hbar\Omega > \frac{\gamma_{SP}}{\sqrt{2(1+\gamma_0/2\gamma_{SP})}} = 99$ meV, is considered to be the more appropriate criterion.[21,50] Then in Figure 3c, the hybrid nanocavity composed of particles >71 nm achieved strong coupling. Note that photoluminescence (PL) measurement is more accurate for understanding the difference between strong and weak coupling.[51–55] However, obvious

splitting characterized by PL, especially at zero detuning, is still a big challenge in hybrid nanocavities.

3. Conclusion

In summary, we propose a method for directly characterizing the exciton-plasmon coupling based on a photosensitive plasmonic nanocavity. Under the illumination of UV light, the LSPR peaks of the nanocavity can be continuously tuned relative to the exciton wavelength (610 nm, WS_2 monolayer). Therefore, the energy dispersion curves of plexcitons in an individual nanocavity can be achieved directly. Compared with the traditional statistical method based on multiple nanocavities, the fitting accuracy of this method is significantly improved from 0.77 to 0.98. Furthermore, it is found that the coupling strength is linearly increased with the particle size, indicating the real-time tuning of Rabi splitting energy from weak coupling ($\hbar\Omega$ = 65 meV, 55 nm) to strong coupling regime ($\hbar\Omega$ = 170 meV, 92 nm). In addition, the strong coupling criterion is optimized with the synergistic contribution of single-particle absorption and scattering spectra. Thus, this new hybrid platform provides an in situ and all-optical approach for studying the light-matter interaction, thereby opening exciting opportunities for room temperature plexciton manipulations, such as quantum information processing and low-threshold laser.

Supporting Information

Supporting Information is available from the Wiley Online Library or from the author.

Acknowledgements

X.H. and Z.H. contributed equally to this work. This work was supported by the Basic and Applied Basic Research Major Program of Guangdong Province (No.2019B030302003), the National Natural Science Foundation of China (Nos. 12274157, 12274334, 91850113, 12021004, and 11904271), and the Natural Science Foundation of Hubei Province of China (Nos. 2022CFB179, 2023AFA076). Special thanks are given to the Analytical and Testing Center of HUST and the Center of Micro−Fabrication and Characterization (CMFC) of WNLO for use of their facilities.

Conflict of Interest

The authors declare no conflict of interest.

Data Availability Statement

The data that support the findings of this study are available from the corresponding author upon reasonable request.

Keywords

photochromic molecules, plasmonic nanocavity, real-time tuning, single-particle spectroscopy, strong coupling

Received: July 1, 2023
Revised: September 17, 2023
Published online: October 15, 2023

[1] H. Wei, X. Yan, Y. Niu, Q. Li, Z. Jia, H. Xu, *Adv. Funct. Mater.* **2021**, *31*, 2100889.
[2] Q. You, Z Li, Y. Li, L. Qiu, X. Bi, L. Zhang, D. Zhang, Y. Fang, P. Wang, *ACS Appl. Mat. Interfaces* **2022**, *14*, 23756.
[3] H. Chen, Z. Jiang, H. Hu, B. Kang, B. Zhang, X. Mi, L. Guo, C. Zhang, J. Li, J. Lu, L. Yan, Z. Fu, Z. Zhang, H. Zheng, H. Xu, *Nat. Photonics* **2022**, *16*, 651.
[4] J. Sun, Y. Li, H. Hu, W. Chen, D Zheng, S. Zhang, H. Xu, *Nanoscale* **2021**, *13*, 4408.
[5] R. Sáez-Blázquez, Á. Cuartero-González, J. Feist, F. J. García-Vidal, A. I. Fernández-Domínguez, *Nano Lett.* **2022**, *22*, 2365.
[6] C. Tserkezis, A. I. Fernández-Domínguez, P. A. D. Gonçalves, F. Todisco, J. D. Cox, K. Busch, N. Stenger, S. I. Bozhevolnyi, N. A. Mortensen, C. Wolff, *Rep Prog Phys* **2020**, *83*, 082401.
[7] J. Zhao, A. Fieramosca, R. Bao, W. Du, K. Dini, R. Su, J. Feng, Y. Luo, D. Sanvitto, T. C. H. Liew, Q. Xiong, *Nat. Nanotechnol.* **2022**, *17*, 396.
[8] K. Wang, M. Seidel, K. Nagarajan, T. Chervy, C. Genet, T. Ebbesen, *Nat. Commun.* **2021**, *12*, 1486.
[9] Y. Tang, Y. Zhang, Q. Liu, K Wei, X. Cheng, L. Shi, T. Jiang, *Light: Sci. Appl.* **2022**, *11*, 94.
[10] M. Hertzog, M. Wang, J. Mony, K. Börjesson, *Chem. Soc. Rev.* **2019**, *48*, 937.
[11] X. Liu, J. Yi, S. Yang, E.-C. Lin, Y.-J. Zhang, P. Zhang, J.-F. Li, Y. Wang, Y-H. Lee, Z.-Q. Tian, X. Zhang, *Nat. Mater.* **2021**, *20*, 1210.
[12] B. Munkhbat, D. G. Baranov, A. Bisht, M. A. Hoque, B. Karpiak, S. P. Dash, T. Shegai, *ACS Nano* **2020**, *14*, 1196.
[13] B. Chakraborty, J. Gu, Z. Sun, M. Khatoniar, R. Bushati, A. L. Boehmke, R. Koots, V. M. Menon, *Nano Lett.* **2018**, *18*, 6455.
[14] B. Lee, W. Liu, C. H. Naylor, J. Park, S. C. Malek, J. S. Berger, A. T. C. Johnson, R. Agarwal, *Nano Lett.* **2017**, *17*, 4541.
[15] S. Lepeshov, M. Wang, A. Krasnok, O. Kotov, T. Zhang, H Liu, T. Jiang, B. Korgel, M. Terrones, Y. Zheng, A. Alú, *ACS Appl. Mat. Interfaces* **2018**, *10*, 16690.
[16] M. Wang, A. Krasnok, T. Zhang, L. Scarabelli, H Liu, Z. Wu, L. M. Liz-Marzán, M. Terrones, A. Alù, Y. Zheng, *Adv. Mater.* **2018**, *30*, 1705779.
[17] A. J. Moilanen, T. K. Hakala, P. Törmä, *ACS Photonics* **2017**, *5*, 54.
[18] H. Wang, A. Toma, H.-Y Wang, A. Bozzola, E. Miele, A. Haddadpour, G. Veronis, F. De Angelis, L. Wang, Q-D. Chen, H.-L. Xu, H.-B Sun, R. P. Zaccaria, *Nanoscale* **2016**, *8*, 13445.
[19] X. Xiong, Y. Lai, D. Clarke, N. Kongsuwan, Z. Dong, P. Bai, C. E. Png, L. Wu, O. Hess, *Adv. Opt. Mater.* **2022**, *10*, 2200557.
[20] X. Yan, H. Wei, *Nanoscale* **2020**, *12*, 9708.
[21] J.-Y Li, W. Li, J. Liu, J. Zhong, R. Liu, H. Chen, X.-H. Wang, *Nano Lett.* **2022**, *22*, 4686.
[22] L. Yang, X. Xie, J. Yang, M. Xue, S. Wu, S. Xiao, F. Song, J. Dang, S. Sun, Z. Zuo, J. Chen, Y. Huang, X. Zhou, K. Jin, C. Wang, X. Xu, *Nano Lett.* **2022**, *22*, 2177.
[23] M. Geisler, X. Cui, J. Wang, T. Rindzevicius, L. Gammelgaard, B. S. Jessen, P. A. D. Gonçalves, F. Todisco, P. Bøggild, A. Boisen, M. Wubs, N. A. Mortensen, S. Xiao, N. Stenger, *ACS Photonics* **2019**, *6*, 994.
[24] M. Pelton, S. D. Storm, H. Leng, *Nanoscale* **2019**, *11*, 14540.
[25] M. Stührenberg, B. Munkhbat, D. G. Baranov, J. Cuadra, A. B. Yankovich, T. J. Antosiewicz, E. Olsson, T. Shegai, *Nano Lett.* **2018**, *18*, 5938.
[26] J. T. Hugall, A. Singh, N. F. Van Hulst, *ACS Photonics* **2018**, *5*, 43.
[27] X. Han, K. Wang, X. Xing, M. Wang, P. Lu, *ACS Photonics* **2018**, *5*, 3970.
[28] X. Han, F. Li, Z. He, Y. Liu, H. Hu, K. Wang, P. Lu, *Nanophotonics* **2022**, *11*, 603.
[29] J. Wen, H. Wang, W. Wang, Z. Deng, C. Zhuang, Y Zhang, F. Liu, J. She, J. Chen, H. Chen, S. Deng, N. Xu, *Nano Lett.* **2017**, *17*, 4689.

[30] J. Cuadra, D. G. Baranov, M. Wersäll, R. Verre, T. J. Antosiewicz, T. Shegai, *Nano Lett.* **2018**, *18*, 1777.
[31] D Zheng, S. Zhang, Q. Deng, M. Kang, P. Nordlander, H. Xu, *Nano Lett.* **2017**, *17*, 3809.
[32] J. Sun, H. Hu, D Zheng, D. Zhang, Q. Deng, S. Zhang, H. Xu, *ACS Nano* **2018**, *12*, 10393.
[33] S. Hou, L. Y. M. Tobing, X. Wang, Z. Xie, J. Yu, J. Zhou, D. Zhang, C. Dang, P. Coquet, B. K. Tay, M. D. Birowosuto, E. H. T. Teo, H. Wang, *Adv. Opt. Mater.* **2019**, *7*, 1900857.
[34] X. Chen, Y. Yang, Y-H. Chen, M. Qiu, R. J. Blaikie, B. Ding, *J. Phys. Chem. C* **2015**, *119*, 18627.
[35] C. Ciracì, X. Chen, J. J. Mock, F. Mcguire, X. Liu, S.-H. Oh, D. R. Smith, *Appl. Phys. Lett.* **2014**, *104*, 023109.
[36] W. M. Wilson, J. W. Stewart, M. H. Mikkelsen, *Nano Lett.* **2018**, *18*, 853.
[37] T. Ming, L. Zhao, M. Xiao, J. Wang, *Small* **2010**, *6*, 2514.
[38] C. Zhang, D. Li, G. Zhang, X. Wang, L Mao, Q. Gan, T. Ding, H. Xu, *Sci. Adv.* **2022**, *8*, eabj9752.
[39] D. Liu, Y. Wang, Q. Zhang, Y. M. Qing, Y. Wang, H. Huang, C. W. Leung, D. Lei, *Nano Lett.* **2023**, *23*, 5851.
[40] A.-L. Baudrion, A. Perron, A. Veltri, A. Bouhelier, P.-M. Adam, R. Bachelot, *Nano Lett.* **2013**, *13*, 282.
[41] L. Lin, M. Wang, X. Wei, X. Peng, C. Xie, Y. Zheng, *Nano Lett.* **2016**, *16*, 7655.
[42] J. A. Hutchison, T. Schwartz, C. Genet, E. Devaux, T. W. Ebbesen, *Angew. Chem., Int. Ed.* **2012**, *51*, 1592.
[43] J. M. Taskinen, A. J. Moilanen, H. Rekola, K. Kuntze, A. Priimagi, P. Törmä, T. K. Hakala, *ACS Photonics* **2020**, *7*, 2850.
[44] F. Benz, R. Chikkaraddy, A. Salmon, H. Ohadi, B. De Nijs, J. Mertens, C. Carnegie, R. W. Bowman, J. J. Baumberg, *J. Phys. Chem. Lett.* **2016**, *7*, 2264.
[45] R. Chikkaraddy, B. De Nijs, F. Benz, S. J. Barrow, O. A. Scherman, E. Rosta, A. Demetriadou, P. Fox, O. Hess, J. J. Baumberg, *Nature* **2016**, *535*, 127.
[46] R. K. Yadav, M. R. Bourgeois, C. Cherqui, X. G. Juarez, W. Wang, T. W. Odom, G. C. Schatz, J. K. Basu, *ACS Nano* **2020**, *14*, 7347.
[47] Q. Zhao, W.-J. Zhou, Y.-H. Deng, Y-Q. Zheng, Z.-H. Shi, L. Kee Ang, Z.-K. Zhou, L. Wu, *J. Phys. D: Appl. Phys.* **2022**, *55*, 203002.
[48] Z. Yuan, S.-H. Huang, Z. Qiao, C. Gong, Y. Liao, M. Kim, M. D. Birowosuto, C. Dang, P. C. Wu, Y-C. Chen, *Laser Photonics Rev.* **2022**, *16*, 2200016.
[49] R. Du, H. Hu, T. Fu, Z. Shi, S. Zhang, H. Xu, *Nano Lett.* **2023**, *23*, 444.
[50] R. Liu, Z. Liao, Y-C. Yu, X.-H. Wang, *Phys. Rev. B* **2021**, *103*, 235430.
[51] M. Wersäll, B. Munkhbat, D. G. Baranov, F. Herrera, J. Cao, T. J. Antosiewicz, T. Shegai, *ACS Photonics* **2019**, *6*, 2570.
[52] J. Qin, Y-H. Chen, Z. Zhang, Y. Zhang, R. J. Blaikie, B. Ding, M. Qiu, *Phys. Rev. Lett.* **2020**, *124*, 063902.
[53] M. Wersäll, J. Cuadra, T. J. Antosiewicz, S. Balci, T. Shegai, *Nano Lett.* **2017**, *17*, 551.
[54] Y. Jiang, H. Wang, S. Wen, H. Chen, S. Deng, *ACS Nano* **2020**, *14*, 13841.
[55] H. Leng, B. Szychowski, M.-C. Daniel, M. Pelton, *Nat. Commun.* **2018**, *9*, 4012.